

# The Low End of the Initial Mass Function in Young LMC Clusters: I. The Case of R136<sup>1</sup>

Marco Sirianni<sup>2,3</sup>, Antonella Nota<sup>3,4</sup>, Claus Leitherer<sup>3</sup>, Guido De Marchi<sup>5</sup>,  
and Mark Clampin<sup>3</sup>

To appear in *The Astrophysical Journal*

---

<sup>1</sup>Based on observations with the NASA/ESA *Hubble Space Telescope*, obtained at the Space Telescope Science Institute, which is operated by AURA for NASA under contract NAS5-26555, and observations obtained at the European Southern Observatory, La Silla.

<sup>2</sup>The Johns Hopkins University: sirianni@pha.jhu.edu

<sup>3</sup>Space Telescope Science Institute, 3700 San Martin Drive, Baltimore, MD 21218; nota@stsci.edu, leitherer@stsci.edu, clampin@stsci.edu.

<sup>4</sup>Affiliated with the Astrophysics Division, Space Science Department of the European Space Agency.

<sup>5</sup>European Southern Observatory: gdmarchi@eso.org

Received \_\_\_\_\_; accepted November 28, 1999

## ABSTRACT

We report the result of a study in which we have used very deep broadband V and I WFPC2 images of the R136 cluster in the Large Magellanic Cloud from the HST archive, to sample the luminosity function below the detection limit of  $2.8 M_{\odot}$  previously reached. In these new deeper images, we detect stars down to a limiting magnitude of  $m_{F555W} = 24.7$  ( $\simeq 1$  magnitude deeper than previous works), and identify a population of red stars evenly distributed in the surrounding of the R136 cluster. A comparison of our color-magnitude diagram with recently computed evolutionary tracks indicates that these red objects are pre-main sequence stars in the mass range  $0.6 - 3 M_{\odot}$ . We construct the initial mass function (IMF) in the  $1.35 - 6.5 M_{\odot}$  range and find that, after correcting for incompleteness, the IMF shows a definite flattening below  $\simeq 2 M_{\odot}$ . We discuss the implications of this result for the R136 cluster and for our understanding of starburst galaxies formation and evolution in general.

*Subject headings:* Magellanic Clouds – stars: evolution – stars: mass function

## 1. Introduction

The quest for a *universal* IMF has been a long standing issue in stellar astrophysics (Scalo 1998). With the advent of the HST and the improved sophistication of ground based instrumentation, it has been possible to extend to nearby galaxies studies that were in the past feasible only in our own Milky Way, and at the same time reach the new domain of the faintest and least massive stars, even before they approach the main sequence. The studies of the IMF have expanded in scope but also triggered new questions and added new uncertainties.

For the field IMF, the uncertainties on distance and star formation can be so huge (Scalo 1998), that it would be difficult to establish local variations. However, there is general agreement that a slightly steeper slope than Salpeter's ( $\Gamma = -1.5 - -1.8$  vs  $\gamma = -1.35$  in the mass range  $1 - 10 M_{\odot}$ ) is generally found. In the case of the IMF for star clusters and associations, the distance effects are removed and the star formation history is simpler. For star clusters, at high masses ( $10 - 100 M_{\odot}$ ) there is good agreement that the Salpeter IMF is ubiquitous. At small and intermediate masses ( $1 - 10 M_{\odot}$ ) the situation is very different. Even in the LMC itself, deep photometry of clusters has produced wildly discrepant results, ranging from the very steep IMFs found by Mateo (1988) ( $\Gamma = -2.52$ ), to the much shallower slopes ( $\Gamma \simeq 0 - -1$ ) derived by Elson et al. (1989) and Hunter et al. (1995, 1996).

30 Doradus in the LMC is the closest extragalactic HII region (Kennicutt 1991). It ideally offers a true laboratory for stellar population studies because of its rich star formation history, and well determined distance. It is the local counterpart to distant starburst galaxies and it has been repeatedly defined as their *Rosetta Stone*. However, the emerging star formation picture is a diverse assembly of results which do not allow a fruitful comparison, let alone an extrapolation to more distant galaxies. The situation becomes even more complicated when one considers independent studies of the same region: for

example, Oey and Massey (1995) derived  $\Gamma = -1.3 \pm 0.2$  for the massive stars in the LMC superbubble LH47, while an independent study by Will et al. (1997) quotes a resulting slope  $\Gamma = -2.1$  in the same range of masses, using the same evolutionary models. However, they then assumed a slope  $\Gamma = -1.3$  for the cluster over the entire mass range investigated. At the smallest masses, the discrepancies are even larger: *are we observing true deviations from the Salpeter IMF*, most likely triggered by local conditions of stellar density or star formation history? Or are we simply dominated by the observational uncertainties, related to the data analysis and interpretation, such as the choice of the evolutionary models or treatment of completeness?

For all these reasons, we have started a systematic study of a number of young clusters in the LMC and in the SMC, at different conditions of stellar density, age and metallicity, with the objective of studying the low end of the stellar IMF and to understand whether at small masses the IMF is constrained by local conditions. The advantage of such a study is to reduce the uncertainties associated with data reduction by establishing a homogeneous data treatment procedure including a unique choice of models. This procedure will be applied to all the clusters in the study, starting from the best known example, R136, which we present in this paper. For this cluster, a number of images exists in the HST archive which could be combined to produce deep images of the cluster, enabling us to reach the low mass limit of  $0.6 M_{\odot}$ .

## 2. Observations and data reduction

Multiple images of the R136 cluster were obtained with the WFPC2 on board the HST in several bandpasses after the first refurbishment mission, as part of the Early Release Observations and of the WFPC2/GTO program. In particular, two sets of images were taken in January 1994 and September 1994 as part of proposals 5589 and 5114, which

contained repeated exposures in the filters F555W and F814W. These filters are described in detail by Biretta (1996) and closely resemble the Johnson V, I filters in their photometric properties. A journal of all observations eventually combined is provided in Table 1. All images were taken with a gain of  $7 \text{ e}^- \text{ ADU}^{-1}$ . In both data sets, the R136 cluster was centered in the Planetary Camera (PC), which has a field of view of  $35'' \times 35''$ , with an effective plate scale of  $0''.045 \text{ pixel}^{-1}$ . The other three WF chips observed flanking fields in 30 Doradus, with the same filter configuration, but a larger field of view of  $75'' \times 75''$  per chip and a plate scale of  $0''.1 \text{ pixel}^{-1}$ .

The two datasets were processed independently using the standard STScI pipeline procedure, which adopts standard calibration observations and reference data, such as bias, flat field, and dark frames constantly updated by the WFPC2 team to track any changes in the performance of the camera and its detectors. The basic steps of the calibration are the correction for the errors introduced by the analog to digital conversion, bias level and bias pixel-to-pixel variations removal, dark image subtraction, flat field image application and shutter shading corrections.

The images taken in January and September, however, were characterized by different temperatures of the CCDs, and, therefore, different charge transfer characteristics. In fact, in March 1994 a significant charge transfer efficiency (CTE) variation had been found in WFPC2, which caused a 10-15 % gradient in the photometric response of the CCDs along the columns of each chip. This effect is due to the partial loss of signal when charge is transferred down the chip during the readout, with the consequence that stars at higher row numbers appear fainter than they would if they were at low row numbers (Holtzman et al. 1995a). A significant reduction to the CTE effect was achieved by cooling down the four CCDs from  $-76$  to  $-88$  °C. The new temperature became operational on April 23 1994, and the CTE stabilised at a  $\sim 4$  % level. In order to account for the difference in CTE

between the two data sets, different corrections were performed: a 12% correction ramp was applied to the  $-76^{\circ}\text{C}$  data (January 1994), and a 4% correction was applied to the  $-88^{\circ}\text{C}$  data (September 1994) in order to bring the charge packets of each pixel to the values they would have had in the absence of the CTE problem.

The images were then registered and combined to remove cosmic rays. A rotation of  $99.85^{\circ}$  was applied to the final image from the first set, which was also shifted in the horizontal and vertical direction by an amount  $(+74.07, +134.73)$ . The combined images,  $670 \times 590$  pixel in size, have an overall exposure time of 1240 sec and 760 sec in the filters F555W and F814W respectively. It should be pointed out that due to the presence of detector read noise, the total combined exposure time is not fully equivalent to the same time in a single image, and will eventually yield a slightly lower S/N. The combined Planetary Camera image for the filter F555W is shown in Figure 1, with the R136 cluster in the center.

### 3. The photometry

Photometry has been performed on both images, using the PSF fitting routines provided within DAOPHOT. The first step in the photometric reduction procedure was to discriminate between *true* stars and spurious objects which might have been introduced by both the alignment procedure and the hot pixels removal. This was done by studying in detail the characteristics of the stellar PSF. We carefully selected by eye a sample of 150 *bona fide* stars in the final F555W image. A statistical study of this sample allowed us to define an appropriate range for the parameters that DAOFIND uses as selection criteria. Two parameters are particularly important: the *roundness*, which allows us to eliminate objects which are too elongated along rows or columns, and the *sharpness*, which eliminates objects whose profile differs largely from a gaussian profile. From our sample of 150 stars

we found mean values of  $0.78 \pm 0.1$  and  $0.045 \pm 0.165$  for the sharpness and roundness, respectively.

We then ran DAOFIND on our data, by conservatively setting the detection threshold at  $4\sigma$  above the local background level, but excluded any object with sharpness and roundness parameters exceeding by more than  $\pm 3\sigma$  the average bona fide values (Figure 2). We inspected the rejected objects and found that almost all of them were noise peaks associated with hot columns, diffraction spikes or highly saturated stars, with a small number being isolated hot pixels and extended objects. Due to the extreme saturation of the central regions, the innermost  $2''$  of the cluster core were excluded from our study.

The list of stars detected in the F555W combined image was then used to identify the stars in the F814W image: 1706 stars were found to be common to both frames. In order to carry out the photometry with the highest accuracy possible, we first performed aperture photometry and measured the stellar flux in a very small aperture (2 pixel radius), selected to match the FWHM of the PSF ( $\simeq 2$  pixel). We measured the background as the mode of the annulus centered on each star with an inner radius of 3 and an outer radius of 7 pixels. We then constructed a sample PSF by combining three moderately bright and isolated stars, located as close as possible to the unsaturated central region of the frame. In order to properly subtract the background it was necessary to carefully evaluate the aperture correction, accounting for the fraction of source light present in the background annulus. Such a correction is derived by assessing how the PSF encircled energy varies as a function of the distance from the peak. For each image we have measured the encircled energy profile for a number of isolated stars and have used these measurements to correct the fluxes derived with aperture photometry.

The procedure of rotation and shift of the two datasets just marginally modified the final PSF FWHM from the original values of 1.51 pixel and 1.32 pixel for the two separate



datasets to 1.76 pixel in the final F555W combined frame. Although this procedure resulted in a slight degradation of the spatial resolution, photometry tests clearly demonstrate this to be much preferable to the alternative of performing photometry on the individual images.

The magnitudes of the individual stars were then determined relative to an aperture of radius  $0''.5$ , and transformations were made to translate the on-orbit system to the WFPC2 photometric system using the calibration provided by Holtzman et al. (1995b). The zeropoints used were 22.48 mag for the F555W filter and 21.60 mag for the F814W band. The original zeropoints were provided for a gain of  $14 \text{ e}^- \text{ ADU}^{-1}$  to which we have added the correction for the different gain adopted in these observations ( $7 \text{ e}^- \text{ ADU}^{-1}$ ) (Holtzman et al. 1995b).

In Figure 3 we report the photometric errors assigned by DAOPHOT to all our measurements: for our study, we discarded all stars with an associated error larger than 0.2 magnitudes in both filters. With this limitation, we find 1604 stars common to both filters, down to a limiting magnitude  $m_{\text{F555W}} = 24.7$ , which is  $\sim 1$  magnitude deeper than the individual frames published by Hunter et al. (1995, 1996). Although we do not include the full photometry in this paper, the complete table is available in electronic form upon request.

#### 4. The Color-Magnitude diagram

We generated an observed color-magnitude diagram (CMD) where  $m_{\text{F555W}}$  is plotted as a function of the  $(m_{\text{F555W}} - m_{\text{F814W}})$  color (Figure 4), which includes all the stars measured in the combined F555W and F814W frames with photometric errors smaller than 0.2 magnitudes. The CMD immediately reveals the presence of two distinct branches, segregated in color at  $(m_{\text{F555W}} - m_{\text{F814W}}) \simeq 1.1$ .

This color segregation is very similar to the effect observed in the CMD of NGC 3603, the galactic clone of R136 (Drissen, 1999). The most likely origin of this effect could be the presence of differential reddening within the cluster, or to the *real* presence of a second population of faint redder stars.

#### 4.1. Differential reddening in R136?

The distribution of gas and dust in the region surrounding R136 is highly inhomogeneous, as can easily be seen in images of the region taken in the light of  $H\alpha$ , [OIII] and [SII] (Scowen et al. 1998). Ideally, the most accurate strategy would be to redetermine the reddening coefficients for each individual star, and indeed Hunter et al. (1995, 1996) had attempted to do so in their recent papers. Unfortunately, the uncertainties associated with their data, as well as the red leak present in the UV filter they adopted, made this task unsuccessful, and they opted instead for the use of ground based measurements by Fitzpatrick & Savage (1984). They eventually attributed the spread in color they observed in their CMD to the use of a single coefficient.

Adopting the same reddening law of Hunter et al. (1995), originally derived by Fitzpatrick & Savage (1984), we have:  $E(B-V) = 0.38$  and  $R_v = 3.4$ . Converted to our filters, this yields  $A_{F555W} = 1.37$ , and  $A_{F814W} = 0.80$ . In Figure 4 we have superimposed such reddening vector on the observed CMD.

There is consensus that differential reddening exists in the R136 region. However, if differential reddening were the cause for the bimodal distribution observed in our CMD, the total amount of absorption needed would be very high. We should in fact assume an extreme value of  $E(B-V) = 0.51$ , and  $R_v = 6.08$ , to match the two observed features. This value, which is reported in Figure 4 for comparison, is more than three times higher than the observed values, and totally inconsistent with the ground based measurements.

We are therefore confident to exclude the possibility of such a high differential extinction and conclude that the observed split in the CMD is most likely intrinsic, and due to the presence of a second population of fainter, redder stars.

#### 4.2. The red population: evidence for pre-main sequence stars?

The position of the red stars in the CMD is consistent with a population of pre-main sequence (PMS) stars, as already suspected by Hunter et al. (1995). In order to establish whether this scenario is correct, we needed to construct isochrones to assign masses to the stars and determine ages for the stellar population. We used isochrones constructed from the stellar evolution models provided by Siess et al. (1997) for PMS evolution. Siess’s tracks offer the choice of different metallicities:  $Z = 0.02, 0.04, 0.005$ . We adopted  $Z = 0.005$  for this study, which closely matches the LMC values of  $Z = 0.008$ .

The stellar models are provided in the  $[\log(L/L_{\odot}) \text{ vs } \log(T_{\text{eff}})]$  plane. In order to convert the information to the WFPC2  $[(m_{\text{F555W}})_o \text{ vs } (m_{\text{F555W}})_o - (m_{\text{F814W}})_o]$  system, we used the model atmospheres of Kurucz (1993) interpolated at metallicity  $Z = 0.005$  and  $g = 4.0$  and the standard STSDAS SYNPHOT software package to reproduce the WFPC2 photometric response. For each isochrone, we assigned to each point in the plane  $(T_{\text{eff}}, \log g)$  the corresponding Kurucz’s atmospheric model and evaluated the intrinsic color  $(m_{\text{F555W}} - m_{\text{F814W}})_o$  of such a point using SYNPHOT. We then converted  $\log(L/L_{\odot})$  into the  $(m_{\text{F555W}})_o$  magnitude adopting a distance modulus of 18.6 (Walborn et al. 1997), and the Bolometric Correction (BC) provided by Bessel et al. (1998) for the same conditions of gravity.

In Figure 5 we show the dereddened CMD of the R136 cluster, where  $(m_{\text{F555W}})_o$  is plotted as a function of  $(m_{\text{F555W}} - m_{\text{F814W}})_o$ . We have superimposed to the CMD the

isochrones corresponding to the PMS evolutionary tracks in the range  $5 \times 10^5 - 5 \times 10^7$  yr. As expected, the observed red population is very well tracked by these PMS isochrones, and most likely consists of low mass stars (down to  $0.6 M_{\odot}$ ) still approaching the main sequence. Their age is found to be in the range between 1 and 10 Myr. In Figure 5 we also show, for comparison, the position of a star of 1.35, 1.5 and  $2 M_{\odot}$  on the various isochrones.

### 4.3. The age of the R136 cluster and the pre-main sequence stars

There is consensus in the published work that the mean age of the R136 cluster is less than  $5 \times 10^6$  yr. Already at the time when the nature of the central object in R136 was still unclear, Savage et al. (1983) and Schmidt-Kaler & Feitzinger (1982) had proposed an age of  $2 \times 10^6$  yr for the *supermassive* central object. With the discovery of WR features in the integrated spectrum of the central region, the age determination increased (Melnick 1985). Later on, Campbell et al. (1992) took high resolution HST/WFPC images of the cluster core, and argued that the presence of WR stars in the central region suggested an age of at least  $3.5 \times 10^6$  yr. Almost at the same time, De Marchi et al. (1993) used the WR stars to place both a lower and upper limit to the age; in fact, while the simple presence of WR stars argues in favour of an age higher than  $2 \times 10^6$  yr, the fact that the WR stars are of the WNL type, a hydrogen rich subclass which is usually associated with very massive progenitors ( $> 50 M_{\odot}$ ), sets a firm upper limit of  $5 \times 10^6$  yr. Such an evidence, combined with the lack of red supergiants found by Campbell et al. (1992), led De Marchi et al. (1993) to conclude in favour of an age determination of  $3 \times 10^6$  yr for the R136 cluster. The most recent work by de Koter et al. (1998) suggests that the WR stars in R136 are younger than classical WNL stars. If so, R136 has an age of at most 2 Myr, and may even be somewhat younger.

In the cluster, star formation is almost coeval: the R136 cluster core extends over a

linear scale  $< 10$  pc. Consider the typical time scale associated with the star formation process ( $t = d/v$ , where  $v$  is the propagation speed of the shock wave triggering star formation). Typical observed values of  $v$  are of order  $50 \text{ km s}^{-1}$  (e.g., Satyapal et al. 1997), so that the possible age spread is less than  $0.5 \text{ Myr}$ . This is small compared to the evolutionary timescale of the stars formed (De Marchi et al. 1993). Outside the R136 cluster, star formation is most likely still continuing (Walborn 1984), especially in the outer filaments of the 30 Doradus region.

If we assume coeval star formation and an age for the cluster of  $\simeq 2 - 4 \times 10^6 \text{ yr}$ , we find that all stars down to  $1 M_{\odot}$  have already reached their birthline, defined as the locus in the HR diagram along which young stars first appear as visible objects (Stahler 1983). In fact, stars of  $1 - 2 M_{\odot}$  reach their birthline in less than  $0.5 \text{ Myr}$ .

As already mentioned, we find that the population of young stars in the R136 CMD is well fitted by isochrones of  $10^6 - 5 \times 10^7 \text{ yr}$ , indicating that we are observing the stars while they are approaching the ZAMS. Typically it takes  $\simeq 5 \times 10^7 \text{ yr}$  for a star of  $1.5 M_{\odot}$  to reach the ZAMS (Siess et al. 1997). This interval is shorter for stars of higher mass. A star of  $2 M_{\odot}$  will take  $\simeq 3 \times 10^7 \text{ yr}$ , and a star of  $3 M_{\odot}$  about  $\simeq 1 \times 10^7 \text{ yr}$ . It is safe to conclude that the red extension of the R136 CMD is made of PMS objects in the  $1-3 M_{\odot}$  range, observed in their approach to the ZAMS.

Did all these stars form at the same epoch of the R136 cluster? As already pointed out by Hunter et al. (1995), stars down to  $3 M_{\odot}$  appear to have formed approximately at the same time of the more massive stars. However, the least massive stars ( $1 - 2 M_{\odot}$ ) could possibly be a few Myr older, but the uncertainties associated with both the theoretical isochrones and the observational data are such that, at this point, no precise answer can be provided.

## 5. The H-R diagram

In an attempt to determine the IMF of R136, we need to locate the stars onto the H-R diagram (HRD). We do so by converting the photometric information (magnitude and color) into the ( $\text{Log } T_{\text{eff}}$  vs  $\text{Log } L/L_{\odot}$ ) plane.

To this purpose, we have used the relation ( $V - I$ ) vs  $T_{\text{eff}}$ , for  $g = 4.0$ , from Bessel et al. (1998). This relation is suitable for PMS stars as well as normal stars (see Sung et al. 1998). From the same source, we also assume BC as a function of  $T_{\text{eff}}$ . In order to use these relations, we have converted  $m_{F555W}$  and  $m_{F814W}$  into  $V$  and  $I$  using the equations provided by Holtzmann et al. (1995b).

We then adopted a distance modulus of  $(m - M)_o = 18.6$  (Walborn et al. 1997) to translate the apparent magnitudes into absolute luminosity, as follows:

$$\text{Log}(L/L_{\odot}) = 0.4 \times (4.75 - M_V - BC)$$

where  $M_V = M_{F555W} - C$ , being  $C$  a correction factor derived for each star from the Holtzmann et al. (1995b). Figure 6 shows the theoretical HRD with the superimposed evolutionary tracks for the mass range  $0.6 - 7 M_{\odot}$  from Siess et al. (1997).

The HRD further illustrates the composition of the intermediate-low mass stellar population in R136 and surroundings: stars with mass above  $4 M_{\odot}$  are already on the main sequence or in close proximity. Stars at lower masses ( $0.6 - 3.0 M_{\odot}$ ) display a higher concentration in proximity to their birth line (at the redward origin of their evolutionary tracks in Figure 6) and have not reached the ZAMS yet. It is interesting to notice that while stars above  $3 M_{\odot}$  evolve at almost constant luminosity to the ZAMS, at smaller masses stars do experience quite significant variations in effective temperature and luminosity, thus creating a quite large observed spread in both quantities. The gap observed at approximately  $T_{\text{eff}} \simeq 3.8 - 3.9$  between the two populations reflects an evolutionary effect. The evolution from the

birth line is faster for high mass stars: stars of  $4 - 7 M_{\odot}$  will transition in that  $T_{eff}$  region much faster than the smallest stars, and therefore they will be observed in smaller numbers, thus creating the observed opening. At the smallest masses ( $1 - 1.5 M_{\odot}$ ), the gap is less noticeable.

### 5.1. The completeness and the photometric errors

Before proceeding to the derivation of the IMF it is also necessary to establish the completeness of our data. With this objective in mind, we have defined four regions (A, B, C, D; see Figure 7) surrounding the R136 cluster in the final combined F555W image. As can be noticed in Figure 7, these four regions have different characteristics in terms of gas/dust contamination and crowding. Region A is the most crowded, and includes many very bright stars, while region C displays some obscurations due to dust and gas. Regions B and D are intermediate in their properties. For each region, and for each filter, the completeness has been assessed with the following procedure:

- The sample of stars falling within the region has been divided into fifteen half magnitude bins;
- Artificial stars have been added to each magnitude bin, in quantity not to exceed 10% of the total number, in order not to affect severely the crowding in the region considered. Numerous tests have been run with the same recipe (100 per bin);
- The artificial stars have been retrieved, using the same selection criteria of sharpness and roundness adopted in our work. Stars with photometric error larger than 0.2 magnitudes have been discarded.

The results of the test are summarized in Table 2, where for each region (A – D) and filter, we have reported the completeness factor as a percentage of the stars successfully retrieved *vs* the total number of stars artificially added. As can be noticed in Table 2, the completeness is worse in the brightest magnitude bin, where saturation effects prevents the detection of other very bright objects, and towards the faint end, where S/N effects start to dominate. In region A, which is characterized by many bright stars, the completeness drops significantly much earlier than for the other regions. For regions B, C, and D the agreement is quite good and the completeness is quite robust (better than 50 %) down to  $m_{F555W} = 23.2$ ,  $m_{F814W} = 22.1$ . We have used an average of regions B, C, and D to derive completeness correction factors for our photometry. We have used the completeness factors determined in this way to draw *completeness lines* onto the HRD to underline the variation of the correction factors with luminosity (Figure 8). As it can be seen in the figure, the completeness is very robust down to  $\text{Log}(L/L_{\odot}) \simeq 0.5$ . In order to understand how this result impacts the definition of a conservative lower mass limit to our measurements, we have constructed in Figure 9, for each of the four regions considered - A,B,C, and D - a completeness histogram as a function of the corresponding mass. As already discussed, regions B, C, and D are in quite good agreement, while region A displays the largest deviation. We have therefore assumed that regions B, C, D are homogeneous in their properties, and we show in Figure 9 their average completeness (solid line). For the average of regions B, C and D we find that the completeness correction drops below 50% at  $\sim 1.35 M_{\odot}$ . This will be the conservative lowest mass limit to our measurements.

Having established the completeness of our photometry, it was necessary to estimate how our photometric errors affect the location of the stars in the HRD and, therefore, the determination of their mass. To this purpose, we have considered four different regions in the CMD, which are representative of different luminosities and temperatures, and sample



the range of values present in our CMD. For each region, we have averaged magnitude and colors for ten stars, in order to derive a single representative point, with a mean magnitude and color. For this representative point, we also derived a mean error, in magnitude and color, as an indication of the uncertainties associated with stars in that region of the CMD. We then transformed these four representative points, and their associated errors, into the HRD (Figure 10), and found that these typical errors on the photometry translate into a small error in luminosity and into a larger error in  $T_{eff}$ . However, since all evolutionary tracks down to  $3 M_{\odot}$  develop at almost constant  $T_{eff}$ , we are confident that such an error in the temperature does not lead to a significant uncertainty in the mass determination, at least for masses higher than  $3 M_{\odot}$ . For masses below  $3 M_{\odot}$ , a translated error of 0.2 in  $\text{Log } T_{eff}$  can affect the mass determination by shifting the star to the adjacent mass bin. This effect increases towards smaller masses, where we should assume an worse case uncertainty on the mass determination of  $\pm 0.3 M_{\odot}$ .

## 6. The Initial Mass Function

### 6.1. The Initial Mass Function of the R136 cluster

The IMF, usually indicated by  $\xi$ , is defined as the number of stars per logarithmic mass interval per unit area. The slope of the IMF is given by  $\Gamma = d(\log\xi)/d(\log M)$  where the standard IMF (Salpeter 1955) has a slope  $\Gamma = -1.35$ . Although we use the term IMF, we are actually discussing the present day mass function (MF). In the case of the very young R136, where star formation has been coeval, we can safely assume that the observed MF is the IMF.

The MF of stellar clusters is usually measured by counting the number of stars as a function of the magnitude (luminosity function) which is then converted into the number

of stars per unit stellar mass by the use of the appropriate mass-luminosity relation. This approach, however, can only be applied to stars currently on their main sequence, i.e. to objects for which a precise correspondence exists between mass and luminosity. As Figure 4 shows, however, R136 hosts a large population of PMS objects, for which such a relation depends strongly on the age and is, therefore, very difficult to apply.

An alternative avenue to follow, which has the advantage of overcoming this age degeneracy, is that presented by Tarrab (1982) and based on the use of the HRD and theoretical isomass tracks in place of the CMD. In order to derive the MF of R136, we have counted the number of stars falling between each pair of tracks shown in the HR diagram (Figure 6) and normalized such number to the width of the mass range spanned by the tracks and to the area of the observed field. As already mentioned, we have adopted the evolutionary tracks by Siess et al.(1997), which also include PMS stars down to  $0.6 M_{\odot}$ . The number of stars in each mass bin is shown in Table 3 (column 3), together with the width of the bin (column 2). To properly account for the effects of crowding, we have corrected the numbers measured in this way for the incompleteness of our photometry, using the *completeness factors* described above (see Table 2). The values corrected in this way are also listed in Table 3 (column 4).

The determination of the MF has been carried out independently in the four regions A, B, C, and D. Since these regions are so differently affected by crowding and dust/gas contamination, and are associated with different completeness corrections, the comparison of their MFs provides an independent assessment of the solidity of our results. Also, we have limited our MF measurements to the magnitude range where the completeness is robust, that is better than 50%. For the average of regions B, C and D the completeness correction drops below 50% at  $\sim 1.35 M_{\odot}$  (see Figure 9). This is the conservative lower mass limit we have assumed for our MF determination.

We find that, within the limitations imposed by small numbers statistics, there is good agreement among the four MFs derived in this way. Following a conservative approach, we have then proceeded to discard the most extreme region (A) (see Figure 9) and have retained only B, C and D for the construction of the final MF, which is shown in Figure 11, where the errors on the data points account for both the Poisson statistics of the counting process and for the uncertainty on the completeness.

Two different trends are distinguishable in the IMF profile of Figure 11: for stars in the mass range  $2.1 - 6.5 M_{\odot}$  the data points are well fit by a slope with  $\Gamma = -1.28 \pm 0.05$ , while at lower masses the IMF profile flattens out, with a derived slope  $\Gamma = -0.27 \pm 0.08$  ( $1.35 - 2.1 M_{\odot}$ ). For comparison, the Salpeter slope is provided on the edge of the figure.

## 6.2. The Mass Function of the surrounding areas of R136

For comparison, we obtained the MF of three flanking fields, which were observed by the three WF chips while the R136 cluster was centered in the field of view of the Planetary Camera. These WF fields covered each a region of  $\simeq 75'' \times 75''$ , and together a total area of  $\simeq 4.7 \text{ arcmin}^2$ . At a distance for the LMC of 52.5 Kpc (Walborn et al. 1997), this corresponds to an area of  $1092 \text{ pc}^2$ . For reference, we provide the central location of all WF chips in Table 4. Since the January and September datasets were taken with different orientations, it was not possible to add the two datasets and reach the same depth as in the combined PC images. Only the September dataset was considered for this work: we reached a magnitude limit in the summed F555W frame of  $m_{F555W} = 24$  with a combined exposure time of 840 s. A total of 2836 stars were found in both filters, selected with the same conservative criterion described above to discard any object with an associated photometric error larger than 0.2 magnitudes in both filters.

A CMD was constructed in similar fashion to what was done for the R136 cluster, and is shown in Figure 12. The most relevant difference from the R136 cluster CMD is a better defined main sequence and the total absence of the second population of red stars. Although the depth of the flanking field images differs from that of the R136 cluster, we can exclude the presence of a second redder population, segregated in color. This can be seen from the insert of Figure 12, which shows the histogram of the number of objects in function of the color ( $m_{F555W} - m_{F814W}$ ) for the R136 cluster (solid line) and the flanking fields (dashed line). The two distributions appear completely different.

The MF was derived following the same procedure described for R136, and the final result is shown in Figure 13. In this case, the filled circles represent our observational data, which are also listed in Table 5 together with the completeness correction factors derived adopting the same procedure. Again, we have used all data points with a photometric completion better than 50%. The MF slope derived in this way is slightly shallower than that of Salpeter, with  $\Gamma = -1.23 \pm 0.11$ .

Can we directly compare the derived MF to the R136 IMF? Naturally, when considering field stars, the additional uncertainty on the distance of the stars considered, and their age, has to be accounted for. Therefore, a direct quantitative comparison cannot be made.

### 6.3. The spatial distribution of the pre-main sequence stars

A first visual inspection of the images indicates that PMS objects are quite uniformly distributed within the field of the Planetary Camera. In order to define more accurately their distribution, we divided the entire field into concentric annuli centered on R136a up to a distance of  $13''$  from the center of the cluster. As already mentioned, we discarded the inner  $2''$  radius region, since the cluster core is highly saturated. We defined each annulus

to be 50 pixels wide, corresponding to  $2''.25$ .

We then compared the spatial distribution, averaged within each annulus, of the PMS stars ( $m_{F555W} - m_{F814W} > 1.1$ ,  $M < 3 M_{\odot}$ ) and of the more massive stars ( $m_{F555W} - m_{F814W} < 1.1$ ,  $M > 3 M_{\odot}$ ). The two distributions are illustrated in Figure 14, where the number of stars per surface area is provided as a function of distance from the cluster center. The solid line with the star symbols indicates the PMS stars and the solid lines with the filled circles the more massive ones.

Both distributions have been corrected for incompleteness. To this purpose, we have performed a second test to establish the completeness level within each annulus, following the same procedure previously described. The results of this test are listed in Table 6, in terms of completeness correction factors for the various annuli. Due to the high number of saturated stars in the central region, we find that the first two annuli (up to  $4.5''$  from the center) are severely affected by incompleteness, and therefore no conclusions can be drawn in the inner cluster regions.

At a distance of  $5''$  from the center and further out, the two distributions are comparable, although the most massive stars display a somewhat steeper decrease in number as we move from the center towards the outer regions of the cluster. The population of pre-main sequence stars appears uniformly distributed in the distance range  $5 - 13''$ , with a very slight increase towards the central regions.

## 7. On the universality of the IMF

The IMF of R136 has been recently studied by Hunter et al. (1995, 1996). Their determination agrees well with ours down to  $\sim 3 M_{\odot}$ , where their data are reliable. Below this limit, however, their errors are so large to make the IMF determination tremendously uncertain and, as such, not meaningful. In all cases, the shape of the IMF at masses

larger than  $\sim 3 M_{\odot}$  is compatible with a power law with index  $\Gamma \simeq -1.2$ , extending up to  $\sim 6.5 M_{\odot}$  in our study and all the way to  $\sim 15 M_{\odot}$  in theirs. The agreement with the canonical IMF of Salpeter (1955) is thus preserved (see Figure 11). Our determination of the IMF is consistent with the work of Sagar & Richtler (1991), who have studied the intermediate mass range in five LMC clusters finding an average slope  $\Gamma \simeq -1.1$  in the range  $2 - 12 M_{\odot}$ .

At lower masses, however, our data are clearly different, indicating a flattening or possibly a drop below  $\sim 2 M_{\odot}$  in the logarithmic plane. This does not mean that the number of objects is no longer increasing with decreasing mass, rather that the increase proceeds at a lower pace. Although in principle crowding could be at the origin of this effect, the flattening of the IMF occurs where our photometry is robust, with a completeness better than  $\sim 50\%$ .

A similar effect, i.e. a deficiency of stars in the  $1 - 2 M_{\odot}$  range, is also observed by Hillenbrand (1997) in the Orion Nebula Cluster, although in that case the plateau is followed first by a steep increase between  $0.5 M_{\odot}$  and  $0.2 M_{\odot}$  and then by a clear drop all the way down to the H-burning limit. Although there are several examples of a flat IMF for stars less massive than  $\sim 1 M_{\odot}$  (see e.g. Comeron, Rieke, & Rieke (1996) in NGC 2024 and Scalo (1998) for a review of the IMF in the solar neighborhood), only in  $\rho$  Oph have Williams et al. (1995) found a flat IMF *above*  $1 M_{\odot}$ . The question as to whether the flattening that we observe in R136 is characteristic of this cluster or a general feature cannot therefore be conclusively addressed, and our finding might simply add on to the conclusion of Scalo (1998) that, at least in this mass range, the IMF is far from being uniform in the Universe.

## 8. Conclusions

The main results of this study are:

- We have detected stars with masses as low as  $0.6 M_{\odot}$  in the R136 cluster using archival HST-WFPC2 images. The least massive stars in our study are about 1 mag fainter than stars known from previous work.
- The lowest mass stars in R136 are identified as a population of pre-main-sequence stars from a comparison with Siess et al. (1997) evolutionary models.
- By combining the pre-main-sequence and the main-sequence population, we are able to derive the stellar IMF between  $1.35$  and  $6.5 M_{\odot}$ . The IMF in this mass range does no longer follow a power law but begins flattening below  $\sim 2 M_{\odot}$ .

Should we call the low-mass IMF in R136 peculiar? It would certainly be too simple-minded to assume that the power-law IMF observed in the high-mass range could extend all the way to lower and lower masses. Evidence for a flattening of the IMF at the low-mass end is manifold in the solar neighborhood (Scalo 1998). Yet, this flattening does not normally set in at masses of  $\sim 2 M_{\odot}$ . Observations of both field stars and clusters in the solar neighborhood suggest a flattening around  $0.3 M_{\odot}$ , an order of magnitude lower than in R136. Almost all Galactic clusters for which the low-mass IMF is known are different from R136 in their stellar content: they contain few, if any, massive stars with masses above  $10 M_{\odot}$ . R136, in contrast, has now been shown to contain  $\sim 10^3$  O stars *and* a significant low-mass population.

The Galactic massive-star formation regions NGC3603 and NGC6231 both have IMF determinations based on star counts. Eisenhauer et al. (1998) find no evidence for an IMF flattening in NGC3603 down to about  $1 M_{\odot}$ . Sung, Bessell, & Lee (1998) on the other

hand report a clear deficit of stars with masses below  $2.5 M_{\odot}$  in NGC6231, the center of the Sco OB1 association. At the higher masses, the IMF in NGC6231 is close to Salpeter. R136 and NGC6231 appear to have rather similar IMF over the mass range 1 to  $100 M_{\odot}$ .

Although low-mass stars are clearly forming in R136 (and other Galactic regions of massive-star formation), they do not form with the same frequency as more massive stars. This is reminiscent of the IMF in starburst galaxies, for which a deficit of low-mass stars has been suggested (Rieke 1991). The low-mass end of the starburst IMF is not accessible to direct observations but must be inferred dynamically. Therefore uncertainties are large and alternative interpretations have been proposed (e.g., Satyapal et al. 1997). The low-mass end of the R136 IMF is not completely dissimilar to an IMF truncated at a few solar masses. The total masses in stars following our derived IMF is very close to the mass obtained from a power-law IMF with a Salpeter slope ( $\Gamma = -1.35$ ) above  $1 M_{\odot}$  and no stars below that mass. Although not quite as extreme as the “top-heavy” starburst IMF, the R136 IMF may indicate a real difference in the mass spectrum of stars formed in- and outside starbursts, possibly related to the gas density of the interstellar medium.



## REFERENCES

- Bessel, M.S., Castelli, F. & Plez, B. 1998, A&A 333, 231.
- Biretta, J. 1996, WFPC2 Instrument Handbook, STScI.
- Campbell, B., Hunter, D.A., Holtzman, J.A., Lauer, T.R., Shayer, E.J., Code, A., Faber, S.M., Groth, E.J., Light, R.M., Lynds, R., O’Neil, J.Jr., Westphal, J.A. 1992, AJ 104, 1721.
- Comeron, F., Rieke, G.H. & Rieke, M.J. 1996, ApJ 463, 294.
- De Marchi, G., Nota, A., Leitherer, C., Ragazzoni, R. & Barbieri, C. 1993, ApJ 419, 658.
- Drissen, L. 1999 in *Wolf Rayet Phenomena in Massive Stars and Starburst Galaxies* ed. K.A. Van der Hucht, G. Koenigsberger, P.R.J Eenens (IAU Symp. n.193)
- Eisenhauer, F., Quirrenbach, A., Zinnecker, H. & Genzel, R. 1998, ApJ 498, 278.
- Elson, R.A.W., Fall, S.M. & Freeman K.C. 1987, ApJ 323, 54.
- Elson, R.A.W., Fall, S.M. & Freeman K.C. 1989, ApJ 336, 734.
- Fitzpatrick, E.L. & Savage, B.D. 1984, ApJ 279, 578.
- Hillenbrand, L.A. 1997, AJ 114, 198.
- Holtzman, J., Hester, J.J., Casertano, S., Trauger, J.T., Watson, A.M., Ballester, G.E., Burrows, C.J., Clarke J.T., Crisp, D., Evans, R.W., Gallagher, J.S.III, Griffiths, R.E., Hoessel, J.G., Matthews, L.D., Mould, J.R., Scowen, P.A., Stapelfeldt, K.R. & Westphal, J.A. 1995a, PASP 107, 156.
- Holtzman, J.A., Burrows, C.J., Casertano, S., Hester, J.J., S., Trauger, J.T., Watson, A.M., & Worthey G. 1995b PASP 107, 1065.

- Hunter D.A., Shaya E.J., Holtzman J.A., Light R.M., O’Neil E.J.Jr. & Lynds R. 1995, ApJ 448, 179.
- Hunter D.A., O’Neil E.J.JR., Lynds R., Shaya E.J., Groth E.J. & Holtzman J.A. 1996, ApJ 459, L27.
- Johnson, H. 1966 *Ann. Rev. Astron. and Astrophys.*, 4, 193.
- Kennicutt R.C.D. 1991, in *Massive Stars in Starburst* ed. C. Leitherer, N. Walborn, T. Heckman, C. Norman (Cambridge: Cambridge University Press), 157.
- Kurucz, R.L. 1993, CD-ROM, Smithsonian Astrophysical Observatory – Cambridge, MA.
- Mateo M. 1988, ApJ 331, 261.
- Melnick, J. 1985, A&A 153, 235.
- O’Connell, R.W., Gallagher, J.S. & Hunter, D.A. 1994 ApJ, 433, 65.
- Oey, M.S. & Massey, P. 1995 ApJ, 452, 210.
- Palla, F. & Stahler, S.W. 1993, ApJ 418, 414.
- Rieke, G.H. 1991 in *Massive Stars in Starburst* ed. C. Leitherer, N. Walborn, T. Heckman, C. Norman (Cambridge: Cambridge University Press), p.205.
- Sagar R. & Richtler T. 1991, A&A 250, 324.
- Salpeter, E.E. 1955, ApJ 121, 161.
- Satyapal, S., Watson, D.M., Pipher, J.L., Forrest, J., Greenhouse, M.A., Smith H.A., Fischer, J. & Woodwar, C.E. 1997 ApJ 483, 148.
- Savage, B.D., Fitzpatrick, E.L., Cassinelli, J.P. & Ebbets, D.C. 1983, ApJ 273, 597.

- Scalo J. 1998, in *The Stellar Initial Mass Function*, G. Gilmore and D. Howell (Eds.), vol. 142 of 38<sup>th</sup> *Herstmonceux Conference*, San Francisco. ASP Conference Series, p.201.
- Scowen, P.A., Hester, J.J., Sankrit, R., Gallagher, J.S., Ballester, G.E., Burrows, C.J., Clarke, J.T., Crisp, D., Evans, R.W., Griffiths, R.E., Hoessel, J.G., Holtzman, J.A., Krist, J., Mould, J.R., Stapelfeldt, K.R., Trauger, J.T., Watson, A.M., & Westphal, J.A. 1998, AJ 116, 163.
- Siess, L., Fiorentini, M. & Dougados, C. 1997, A&A 324, 556.
- Stahler, S.W. 1983, ApJ 274, 822.
- Sung, H., Bessel, M.S. & Lee, S.W. 1998 AJ 115, 734.
- Tarrab, I. 1982, A&A 109, 285.
- Walborn, N.R. 1984, in *Structure and Evolution of the Magellanic Clouds*, IAU Symp. 108, eds. S.Van der Bergh & K.S. De Boer (Dordrecht: Reidel), p.243.
- Walborn, N.R. & Blades J.C. 1997, ApJS 112, 457.
- Will J.M., Bomans D.J. & Dieball A., 1997, A&AS 123, 455.
- Williams D.M., Comeron F., Rieke G.H. & Rieke M.J. 1995, ApJ 454, 144.

Fig. 1.— Final combined WFPC2 image of the R136 cluster in the F555W filter. The image shows the portion of the field of view of the Planetary Camera ( $30'' \times 27''$ ), where the cluster is centered. The orientation on the sky is indicated in the image.

Fig. 2.— A sample of *bona fide* stars selected by eye has been used to statistically derive the appropriate values for the "sharpness" and "roundness" parameters used by DAOFIND to discern the *true* stars from spurious artifacts.

Fig. 3.— Photometric errors assigned by DAOPHOT to all our measurements. For our study, we have discarded all stars with an associated error larger than 0.2 magnitudes in both filters.

Fig. 4.— Observed Color Magnitude Diagram of R136, for all stars measured in the combined images with associated photometric error smaller than 0.2 in both filters. We have superimposed the reddening vector originally derived by Fitzpatrick & Savage (1984), where  $E(B-V) = 0.38$  and  $R_v = 3.4$ . In order to explain with differential reddening the bimodal distribution observed in our CMD, the total amount of absorption needed would be  $E(B-V) = 0.51$ , and  $R_v = 6.08$ . This value is also reported in the figure for comparison.

Fig. 5.— Dereddened Color Magnitude Diagram of the R136 cluster, to which we have superimposed isochrones corresponding to  $5 \times 10^5 - 5 \times 10^7$  yr. The *red population* is well fitted by pre-main sequence isochrones, and most likely consists of low mass stars still approaching the main sequence. We also show, for comparison, the position of a star of 1.35, 1.5 and 2  $M_\odot$  on the various isochrones.

Fig. 6.— H-R diagram for all the stars observed with photometric errors lower than 0.2 magnitudes. We have superimposed to the HRD the pre-main sequence evolutionary tracks for the mass range 0.6 - 7  $M_\odot$  from Siess et al. (1997). The dashed lines indicate post MS evolution.

Fig. 7.— The final combined image in the F555W filter has been subdivided in four regions surrounding the R136 cluster, with the objective of establishing the completeness of our photometry. The four regions display different characteristics in terms of crowding and/or gas/dust contamination. For each region we indicate nomenclature and size (in ".)

Fig. 8.— H-R diagram for all the stars observed with photometric errors lower than 0.2 magnitudes. We have superimposed to the HRD the *completeness lines* derived from the execution of the completeness test executed on regions B,C and D.

Fig. 9.— A completeness histogram as a function of mass for the four selected regions around the R136 cluster: A, B, C, and D. The average completeness for regions B, C and D, which appear to display homogeneous properties, is drawn as a solid line. The mass corresponding to the conservative limit of 50% for the completeness correction factor has been chosen as the lowest limit to our MF determination. This corresponds to  $M = 1.35 M_{\odot}$ .

Fig. 10.— H-R diagram for all the stars observed, to which we have superimposed the error boxes corresponding to four representative stars (and their associated photometric errors) selected in the CMD. This figure illustrates how the photometric errors propagate in the transformation to the HRD. While the resulting error in the luminosity is small, the photometric error translates into a larger error in  $T_{eff}$ .

Fig. 11.— The IMF for the R136 cluster, obtained by averaging the IMFs for the regions B, C, and D, defined as the number of stars per unit logarithmic mass per square parsec. The full circles indicate the completeness-corrected IMF, while the the open diamonds and the stars indicate the slopes from Hunter et al. (1995, 1996). A Salpeter slope is provided for reference.

Fig. 12.— Color Magnitude Diagram for the combination of three fields flanking the R136 cluster, down to a limiting magnitude  $m_{F555W} = 24$ . The stars included have associated photometric error smaller than 0.2 magnitudes in both filters.

Fig. 13.— The IMF for the R136 cluster flanking fields, obtained from the three adjacent WF chips. The total area investigated is  $\simeq 4.7 \text{ arcmin}^2$ , with a limiting magnitude  $m_{F555W} = 24$ .

Fig. 14.— Spatial distribution for the pre-main sequence stars as a function of distance with respect to the R136 cluster center (crosses) compared with the distribution of the more massive stars (full dots).

Table 1: Journal of *HST*+*WFPC2* Observations

Proposal	Date (UT)	Filter	Exposure Time (sec)	Image Name
5589	January 1994	F555W	200	U25Y0109T
5589	January 1994	F555W	200	U25Y0101T
5589	January 1994	F814W	100	U25Y0207T
5589	January 1994	F814W	100	U25Y0208T
5114	September 1994	F555W	120	U2HK030JT
5114	September 1994	F555W	120	U2HK030KT
5114	September 1994	F555W	120	U2HK030LT
5114	September 1994	F555W	120	U2HK030MT
5114	September 1994	F555W	120	U2HK030NT
5114	September 1994	F555W	120	U2HK030OT
5114	September 1994	F555W	120	U2HK030PT
5114	September 1994	F814W	80	U2HK0317T
5114	September 1994	F814W	80	U2HK0318T
5114	September 1994	F814W	80	U2HK0319T
5114	September 1994	F814W	80	U2HK031AT
5114	September 1994	F814W	80	U2HK031BT
5114	September 1994	F814W	80	U2HK031CT
5114	September 1994	F814W	80	U2HK031DT

Table 2: Completeness correction factor for regions A, B, C and D

$m_{F555W}$	A	B	C	D	$m_{F814W}$	A	B	C	D
17.7	64	68	67	70	16.1	87	90	89	91
18.2	84	88	90	89	16.6	89	89	91	93
18.7	85	85	87	89	17.1	89	91	92	93
19.2	80	83	86	89	17.6	85	87	90	90
19.7	79	81	85	87	18.1	85	87	88	90
20.2	69	76	81	84	18.6	79	84	85	88
20.7	67	75	78	83	19.1	74	81	83	85
21.2	61	71	73	83	19.6	70	72	79	85
21.7	54	67	70	80	20.1	64	75	73	83
22.2	44	57	61	78	20.6	57	65	71	81
22.7	32	50	60	69	21.1	45	62	68	71
23.2	25	43	55	63	21.6	41	53	61	71
23.7	14	37	42	48	22.1	25	45	52	61
24.2	8	19	19	22	22.6	11	17	18	19
24.7	0	3	1	2	23.1	2	6	8	8



Table 3: The IMF for the R136 cluster

Mass ( $M_{\odot}$ )	Bin width ( $M_{\odot}$ )	# stars/bin	corrected # stars/bin
0.650000	0.100000	14	64
0.750000	0.100000	12	181
0.850000	0.100000	20	66
0.950000	0.100000	11	31
1.050000	0.100000	10	76
1.150000	0.100000	15	98
1.250000	0.100000	28	254
1.350000	0.100000	30	70
1.450000	0.100000	43	78
1.550000	0.100000	37	64
1.650000	0.100000	39	60
1.750000	0.100000	34	48
1.850000	0.100000	40	57
1.950000	0.100000	38	51
2.100000	0.200000	63	84
2.350000	0.300000	78	102
2.750000	0.500000	91	116
3.500000	1.000000	92	111
4.500000	1.000000	58	68
5.500000	1.000000	44	53
6.500000	1.000000	20	26

Table 4: Coordinates of the WFPC2 flanking field centers

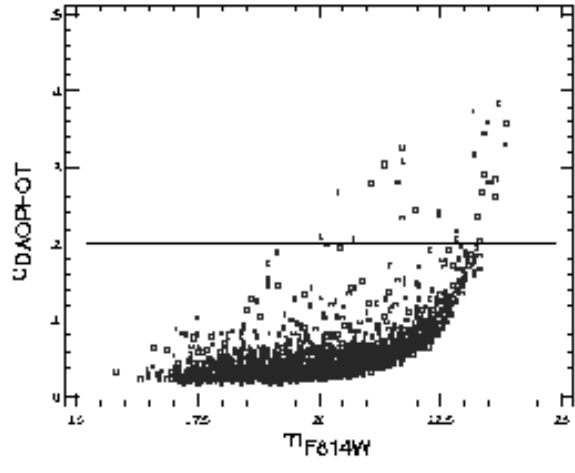
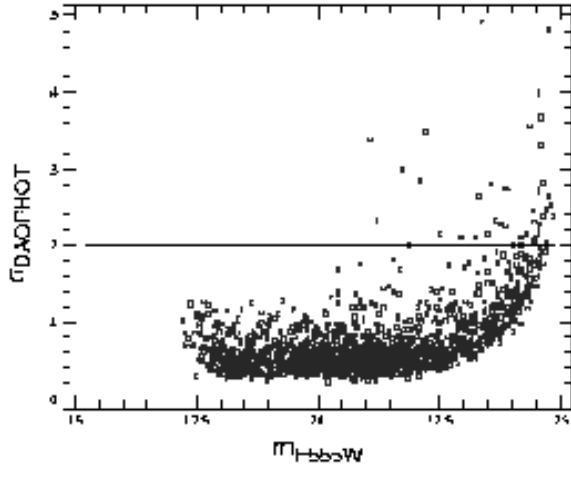
CHIP	R.A.	DEC
WF2	5:38:49.27	-69:05:17.50
WF3	5:38:57.23	-69:06:12.72
WF4	5:38:46.68	-69:06:56.70

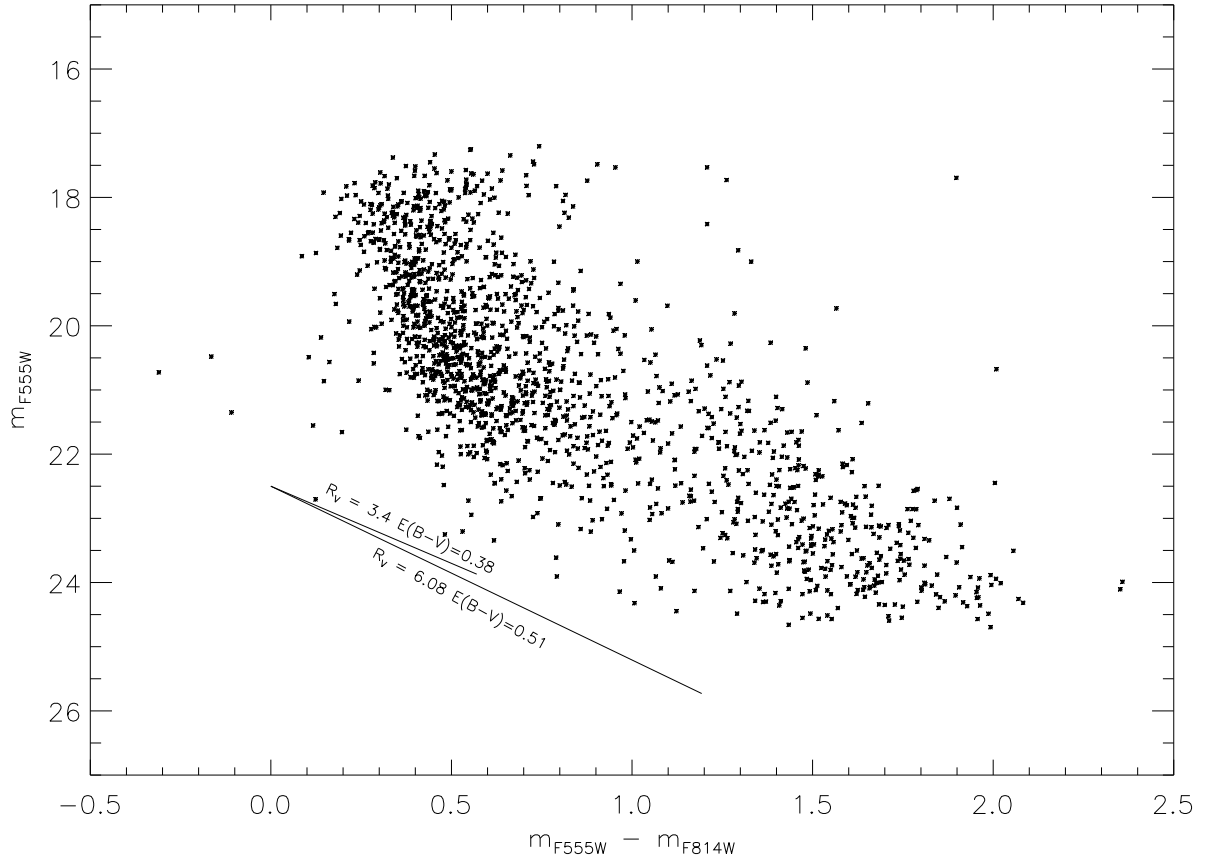
Table 5: The IMF for the Field

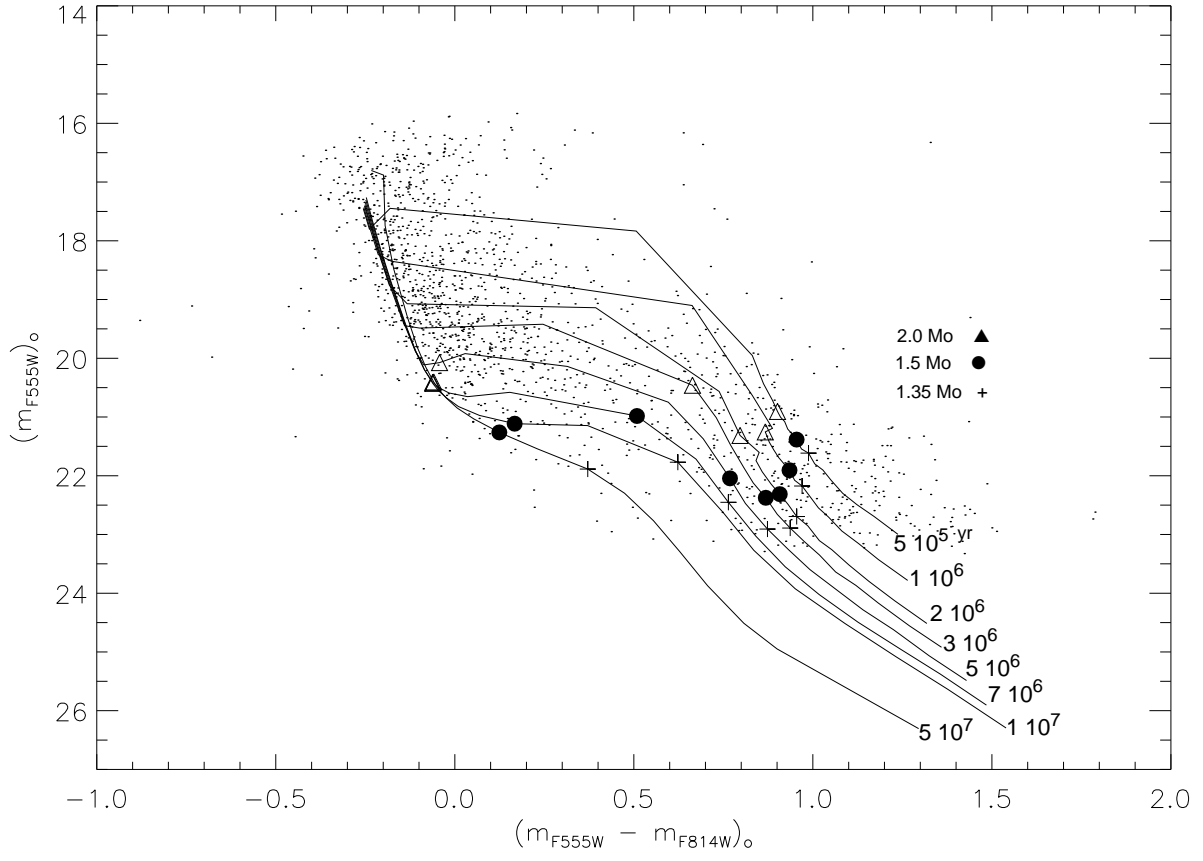
Mass ( $M_{\odot}$ )	Bin width ( $M_{\odot}$ )	# stars/bin	corrected # stars/bin
1.05000	0.100000	2	5
1.15000	0.100000	14	41
1.25000	0.100000	63	626
1.35000	0.100000	179	484
1.45000	0.100000	156	214
1.55000	0.100000	163	195
1.65000	0.100000	176	201
1.75000	0.100000	129	145
1.85000	0.100000	126	143
1.95000	0.100000	104	111
2.10000	0.200000	179	189
2.35000	0.300000	168	176
2.75000	0.500000	258	267
3.50000	1.00000	331	341
4.50000	1.00000	217	222
5.50000	1.00000	108	110
6.50000	1.00000	85	87

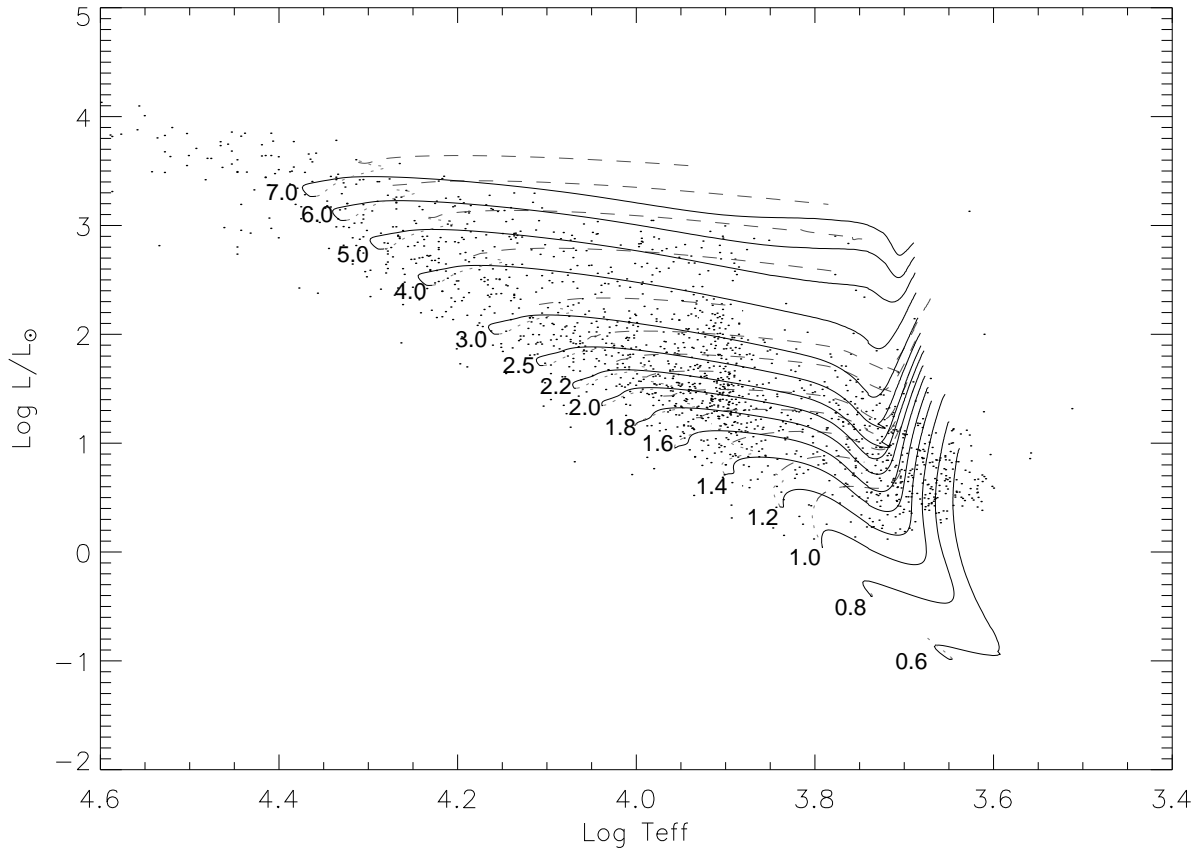
Table 6: Spatial Distribution completeness test

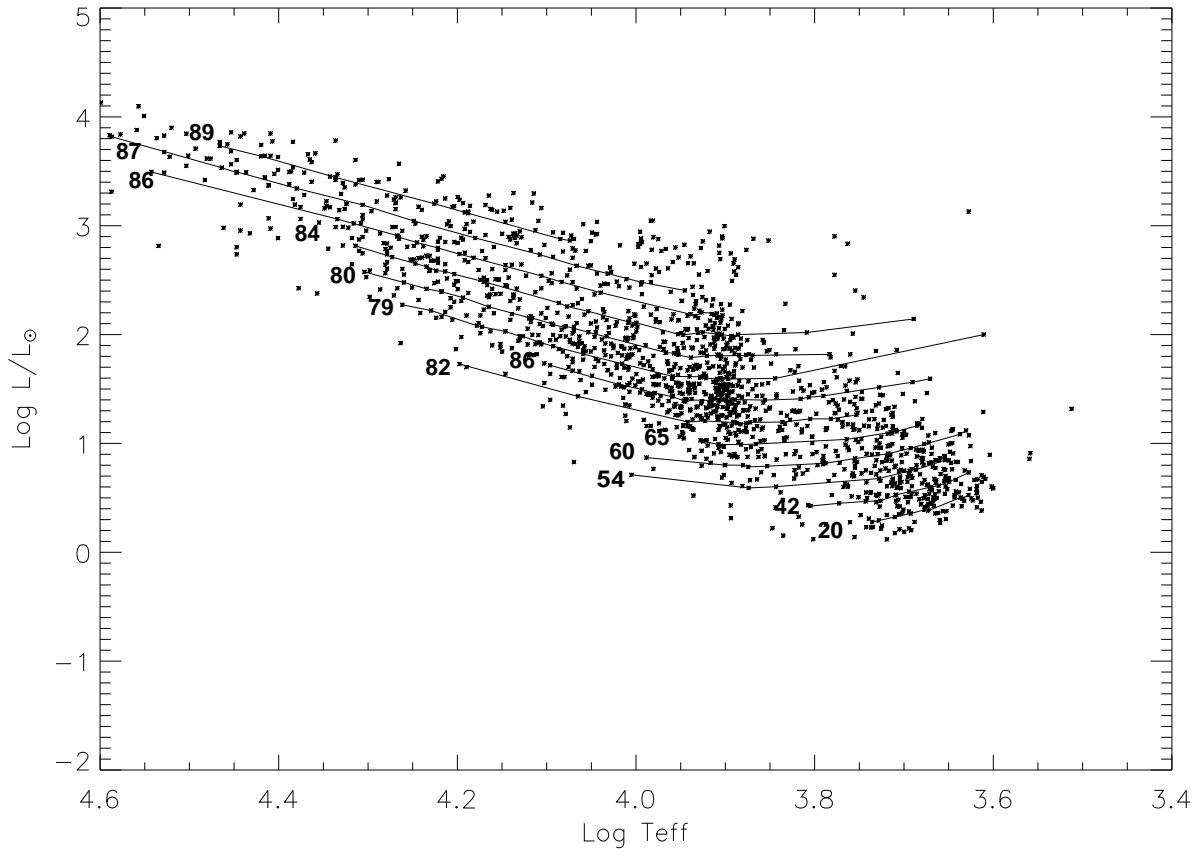
$M_{F555W}$	Distance				
	3.375'	5.625''	7.875''	10.125''	12.375''
17.7	58	64	64	69	73
18.2	77	86	87	90	88
18.7	71	84	86	90	88
19.2	67	80	81	86	88
19.7	56	74	79	84	80
20.2	50	69	72	81	77
20.7	40	62	71	78	74
21.2	31	56	66	70	67
21.7	25	48	61	66	62
22.2	18	42	53	57	59
22.7	9	33	43	51	52
23.2	2	26	35	42	44
23.7	0	18	28	32	32
24.2	0	7	13	14	15
24.7	0	1	2	3	2



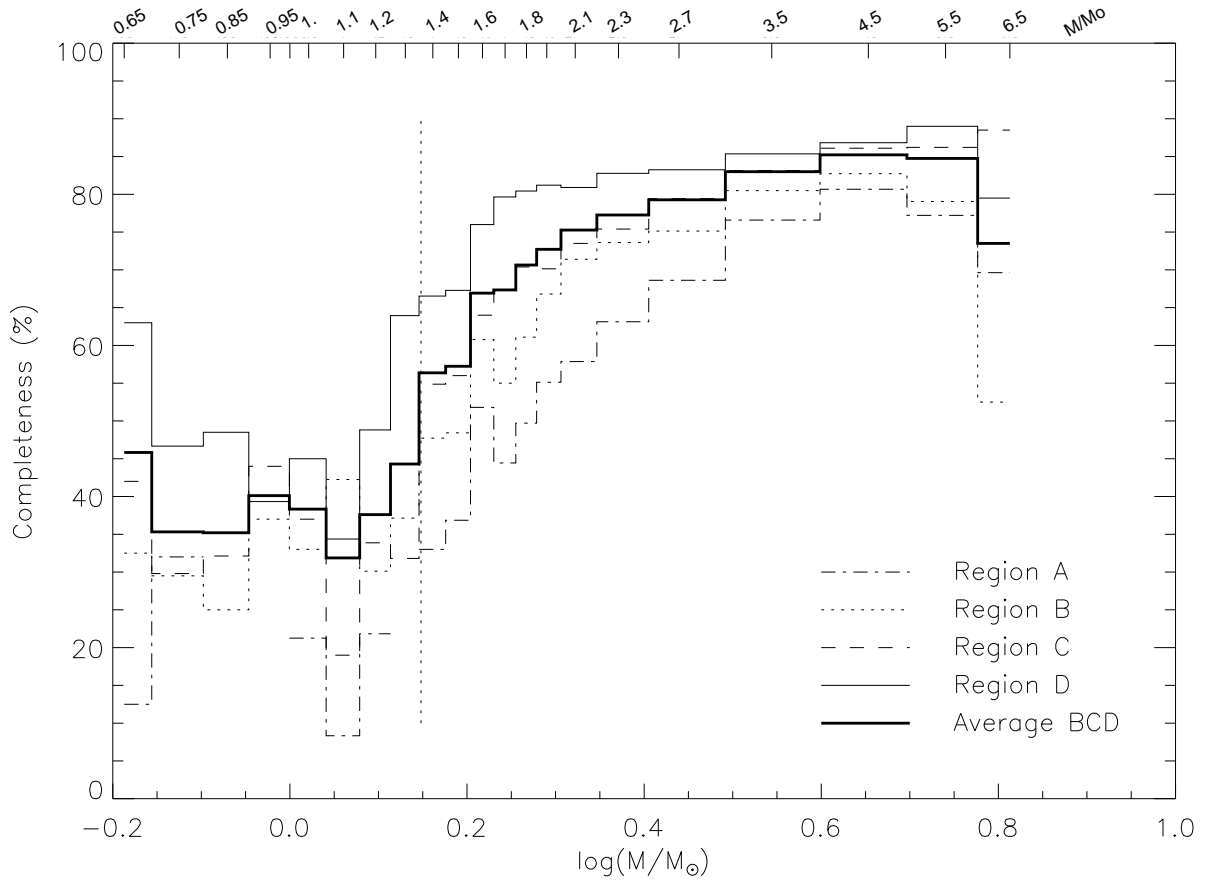


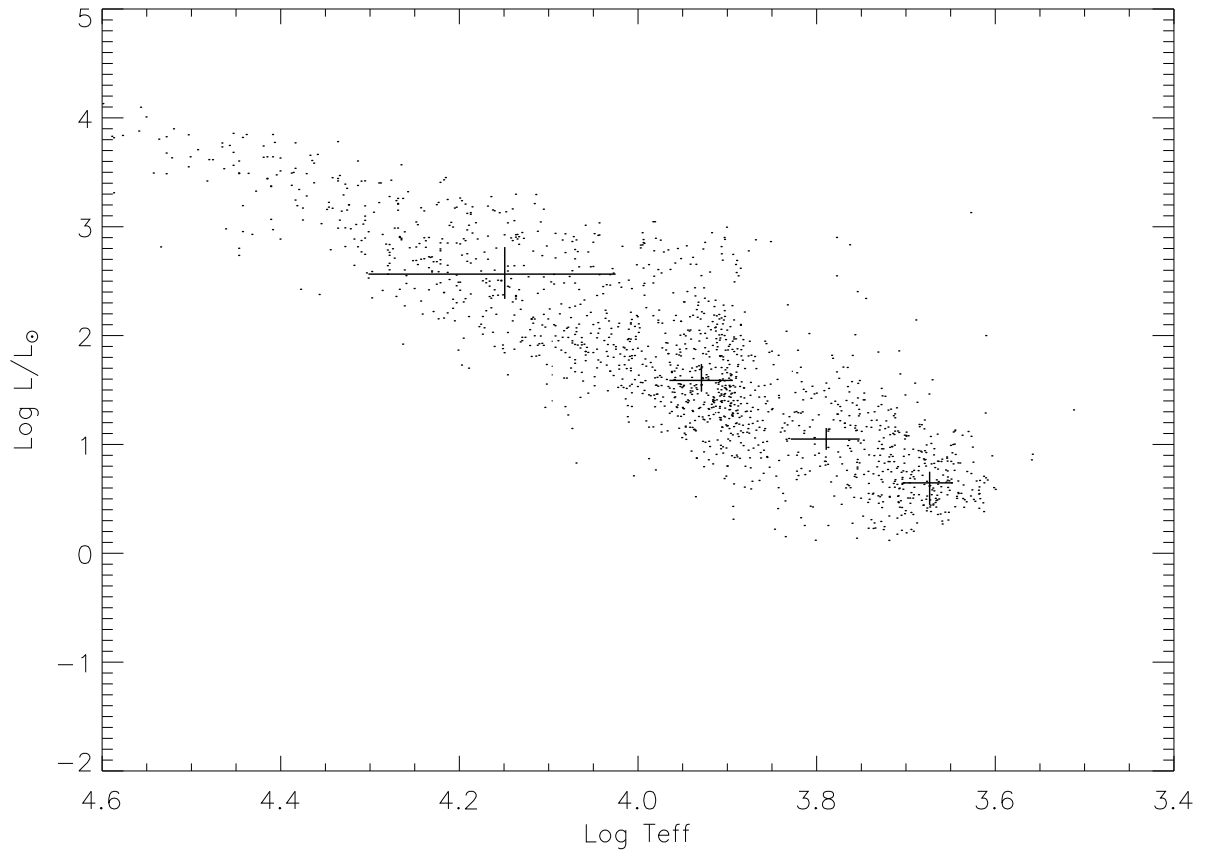


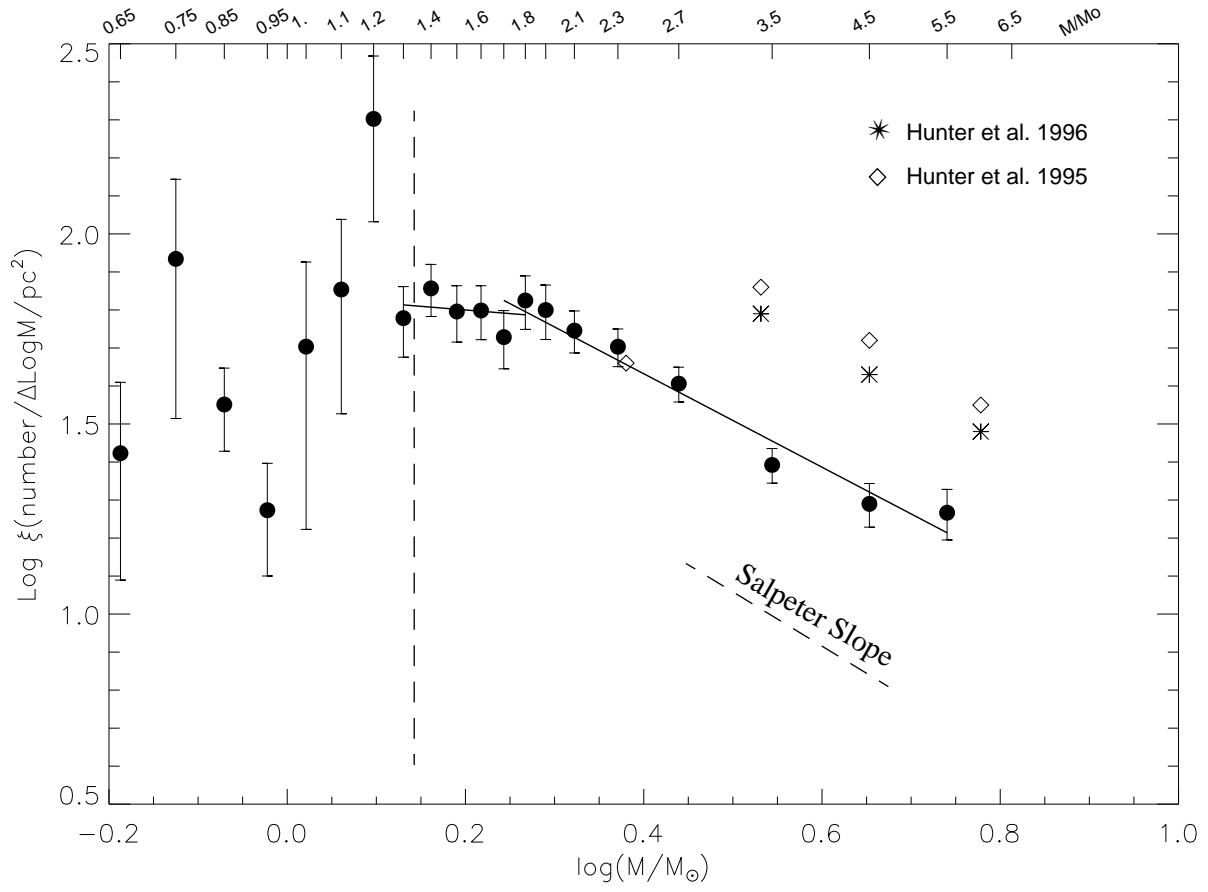


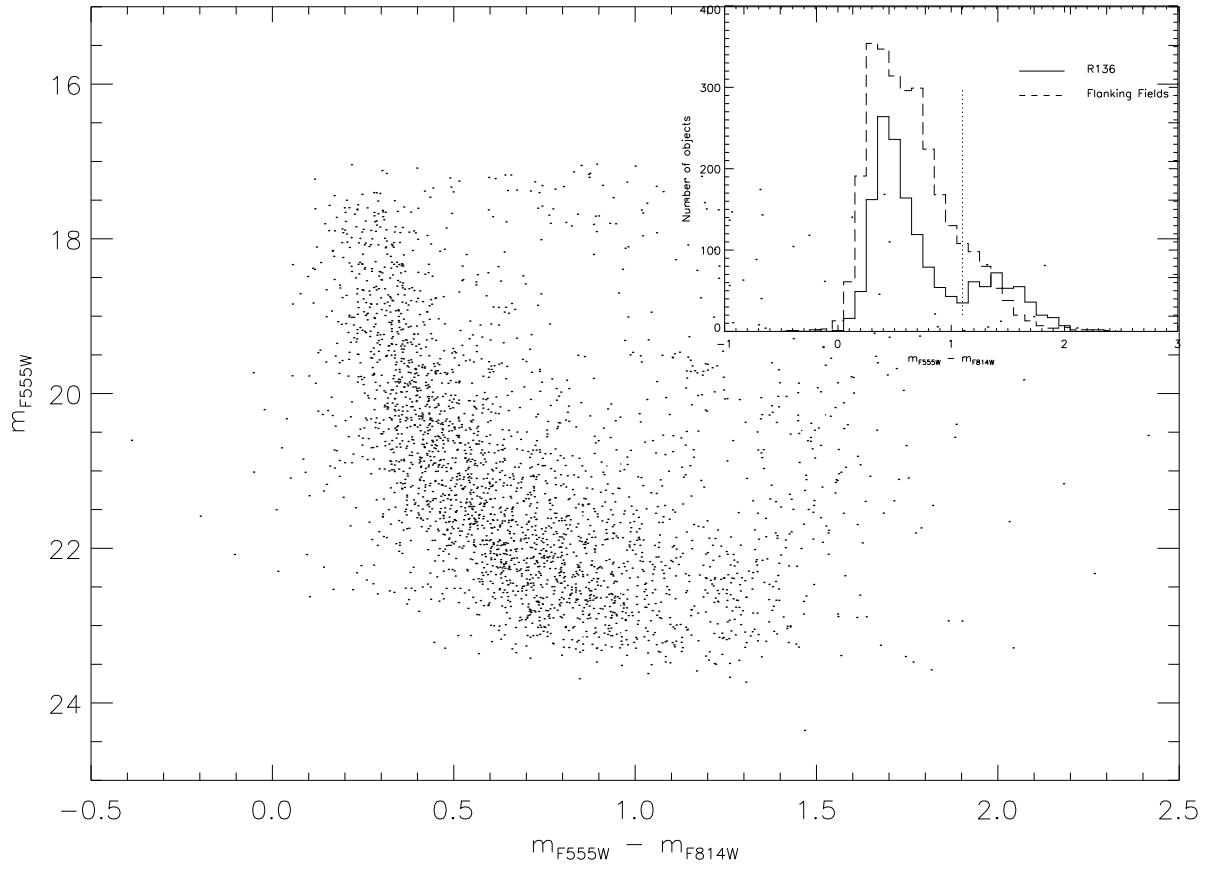


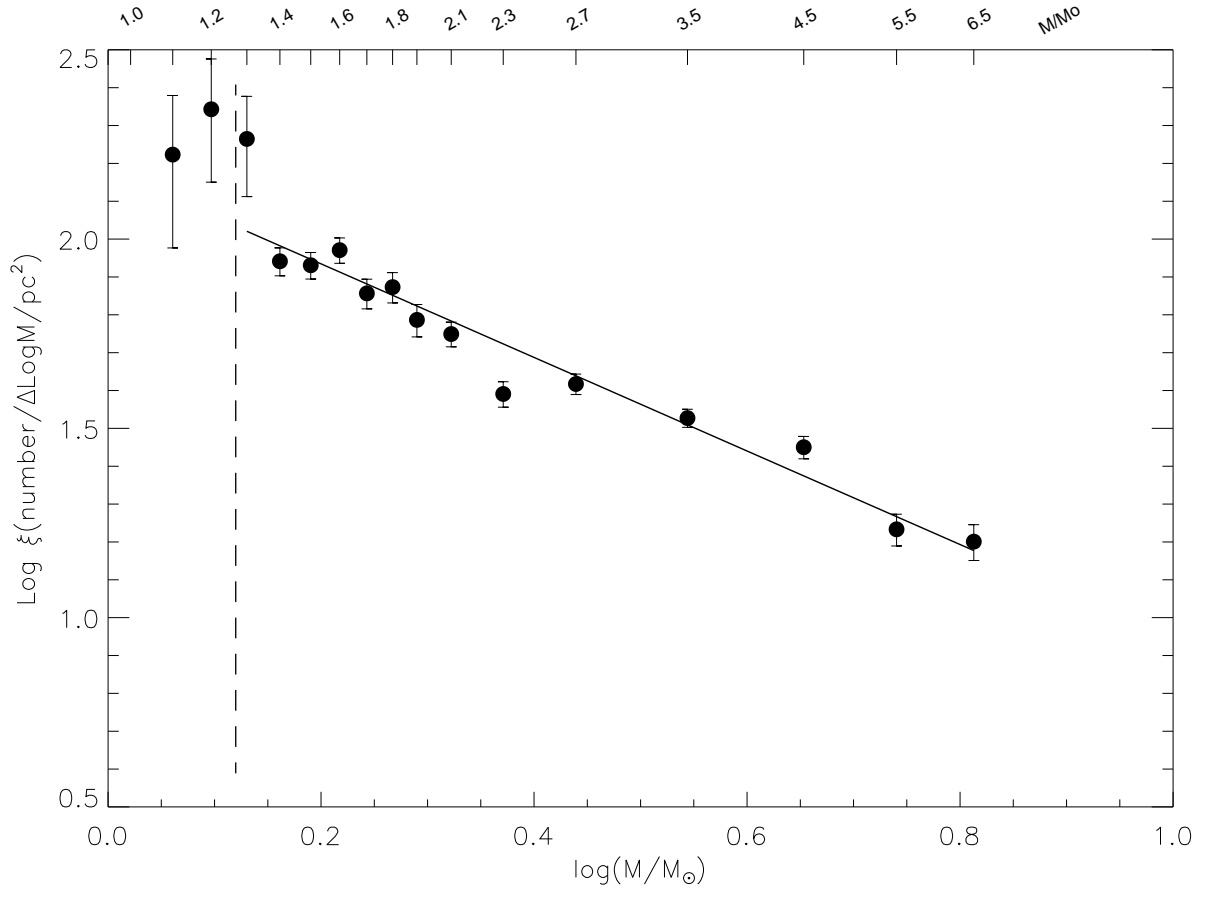


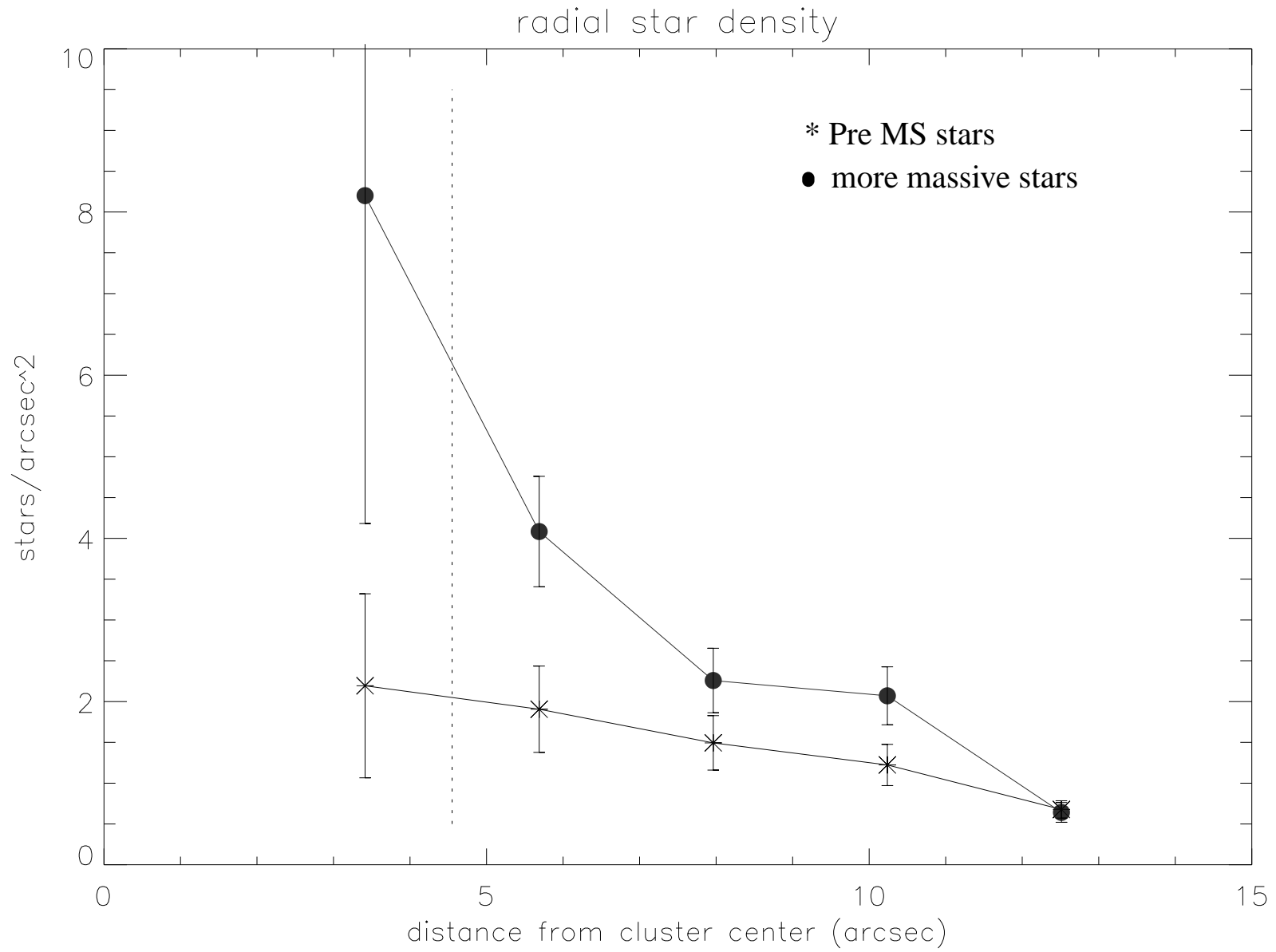












This figure "fig1.jpg" is available in "jpg" format from:

<http://arxiv.org/ps/astro-ph/9911524v1>

This figure "fig2.jpg" is available in "jpg" format from:

<http://arxiv.org/ps/astro-ph/9911524v1>



This figure "fig7.jpg" is available in "jpg" format from:

<http://arxiv.org/ps/astro-ph/9911524v1>